A Novel ES-RwCNN Based Finger Vein Recognition System with Effective L12 DTP Descriptor and AWM-WOA Selection

Ajai Kumar Gautam*, Rajiv Kapoor

***Abstract*—Fingerprints, faces, and also irises are Biometrics, which are extensively utilized in several recognition applications comprising door access control, automatic teller machines, personal authentication for computers, Internet banking, along with border-crossing controls with recent augments in security necessities. The unique patterns of finger veins (FV) are utilized by Finger vein recognition (FVR) for detecting individuals at a high-level accuracy. However, on account of the existence of artifacts, irregular shading, distortions, etc., precise FV detection is a difficult task. A framework for identifying FV is created by the work to offer a precise biometric authorization utilizing Enhanced Sigmoid Reweighted based Convolutional Neural Network (ES-RwCNN). The image is initially pre-processed by the framework via executing rotation, cropping, resizing, and normalization for avoiding unwilling distortions. Utilizing Trapezoid Membership Function-Based Contrast Limited Adaptive Histogram Equalization (TMF-CLAHE), the pre-processed image is followed with contrast enhancement (CE) that intensifies the image by evading irregular shading and vein posture deformation along with upgrades the accuracy rate. After that, utilizing the Local 12 direction texture pattern (L_{12}DTP) and Canny Edge method, knowledgeable textural and edge features (EF) are extracted. For attaining the most informative features, an Adaptive Weight Mutated Whale Optimization Algorithm (AWM-WOA) technique is formed by the work that enhances the model's accuracy and decreases the computational complexity (CC). Finally, for identifying the authorized person, the chosen features are presented to ES-RwCNN. The work attains a low information loss by achieving a 0.971 correlation betwixt the pre-processed image and the original image (OI), as shown by the experimental analysis. Classification accuracy (CA) of 97.05% is attained by the framework. It avoids misclassification by acquiring a 3.53% False Positive Rate (FPR) and 2.35% False Rejection Rate (FRR). It continues to be comparatively efficient analogized to the existing methods.**

***Index Terms*—Authorization, Biometric, Finger Vein Recognition (FVR), Trapezoid Membership Function-Based Contrast Limited Adaptive Histogram Equalization (TMF-CLAHE), Local 12 direction texture pattern (L12DTP), Adaptive Weight Mutated Whale Optimization Algorithm (AWM-WOA), Enhanced Sigmoid Reweighted based Convolutional Neural Network (ES-RwCNN).**

Manuscript received June 03, 2021; revised April 07, 2022.

Ajai Kumar Gautam is an Assistant Professor in Electronics & Communication Engineering Department at Delhi Technological University, Delhi, India. (phone: +919868244926; e-mail: ajaikumargautam.dtu@gmail.com).

Rajiv Kapoor is a Professor in Electronics & Communication Engineering Department at Delhi Technological University, Delhi, India. (e-mail: rajivkapoor@dce.ac.in.)

I. Introduction

The method of recognizing a person centered upon one's unique physiological or behavioral attributes is called Biometrics [1]. Biometric recognition (BR) approaches are generally categorized into 2 types: (i) extrinsic biometric features like iris, palm print, fingerprint, face, and also (ii) Intrinsic biometric features like palm vein, hand vein, and FV. Extrinsic Biometrics is more vulnerable to faked input, which results in security problems. Since intrinsic modalities are hidden beneath the skin, they are hard to be faked, therefore, safer [2, 3].

Face recognition, fingerprint recognition, along palm print recognition are several BR techniques utilized recently. But, the methods were most susceptible to faked input, spoof attacks, external damages, and impersonation, which produced security issues [5, 6]. For resolving such issues, FVR technology is broadly utilized for human verification. Therefore, owing to its unique identification along with proper authentication, the FVR technology is a suitable BR method [7].

The minute blood vessels inside our fingers that are distinctive to each individual are FV [8]. The blood vessels with hemoglobin are recognizable as a sequence of dark lines while passing infrared images [9]. Only from a living body, FV images could be captured; therefore, if the person is dead, it is impossible to steal the identity. Furthermore, FVR is not influenced by weather or age in the skin. It is comparatively secure and more steady [10]. But, the Computer-Aided Diagnosis (CAD) is utilized for the enhancement of accuracy with a decrease of time in interpreting the images.

Image acquisition (IA), feature extraction (FE), pre-processing, along with matching are the disparate stages for recognizing the FV images in CAD [11]. An Infrared LED light is transmitted via the finger together with attains a higher contrast image in the IA phase [12]. By conducting a few operations, like resizing, scaling, and CE, the information (unnecessary) in the image (input) is eliminated in a pre-processing stage. The major stage in FVR is the FE. Here, as of the image (pre-processed), the most informative features are extracted. For recognizing individuals, it is basically utilized [13]. The final step is matching; here, for checking whether the image (input) is authentic or not, the input's likeness and the enrolled templates are contrasted [14]. But, the FVR was more precise along with it possesses lower FRR along with False Acceptance Rate. It also presents a few drawbacks concerning extracting the FV

patterns from low contrast finger images. It also possesses an image classification issue [15].

For conquering such challenges, Zone-centered Minutia Matching [16], Support Vector Machine and also neural network (NN) method [17], Convolutional NN (CNN) [18], Lightweight CNN (L-CNN) [19], and also Deep learning (DL) methods are the several methods that are presented. Because of poor image restoration, information loss during FE, and reduction, the CA was not efficiently addressed by the scheme, although the prevailing methods possess a higher degree of privacy and higher recognition rate (RR). It also exhibits different problems like a deficit of training data's availability, uncertain image portrayal, misalignment, restricted CE, need high storage space for large templates along with noise amplification [20]. For overcoming such drawbacks, an ES-RwCNN is formed by the work for executing the user data's FV authentication.

This paper is categorized as Section II reviews the different top-notch methods in the FVR. Section III elucidates the proposed work. Section IV demonstrates the results and a discussion aimed at the proposed method centered on performance metrics. Lastly, section V presents the conclusion with future scope.

II. Literature Review

Wenhao You et al. [21] presented a bilayer restoration technique that dealt with skin scattering along with enhancing the FV image's visibility. The inherent factors were also examined that caused the FV image's degradation. Hence, the scheme enhanced the blurred image's clarity, enhanced the venous network, and was more dependable in FV image restoration. Concerning robustness and restoration performance, the method had surpassed the other techniques, as shown by the investigational outcomes. However, it possessed a noisy data drawback.

CihuiXie et al. [22] presented a method intended for the FV authentication centered on CNN and also supervised discrete hashing (SDH). The SDH's inclusion as of a CNN had attained the most precise performance, which utilized the triplet-centered loss function. Superior outcomes over other deemed CNN architecture were attained by means of the proposed work and also proffered a considerably decreased template size. However, low accuracy rates were shown by the scheme.

Tong Liu et al. [23] introduced a Direction-Variance-Boundary Constraint Search model and reinstated the broken FV patterns. Broken branches of FV patterns were not only effectively restored by the scheme but also enhanced the FVR's performance drastically. The scheme decreased the FVR's error rate from 0.57% to 0.29%, as exhibited by the investigational outcome, but it had a drawback of time consumption.

Ismail Boucherit et al. [24] formed an enhanced deep network called Merge CNN that utilized numerous CNN with shorter paths. The augmented RR with more precise identification was the method's major aim. The scheme competed with top-notch methods with a 99.56% RR, as shown by the experimentation outcome. However, it had a drawback of lower image quality.

Weili Yang et al. [25] developed a lightweight CNN named the FVR and Anti Spoofing Network (FVRAS-Net), which incorporated the recognition task together with the anti-spoofing task on a merged CNN by the Multi-Task Learning approach's usage. The more instructive image for FV identification was automatically chosen by the scheme, which efficiently enhanced the recognition performance. Furthermore, greater security along with strong real-time performance was attained by the scheme. Therefore, outstanding performance in recognition and also anti-spoofing tasks was attained by the technique as illustrated by the experiments. But, there prevailed a data scaling drawback.

Tao Zhan et al. [26] created a scheme centered on FV patterns, which utilized block uniform local binary patterns along with block 2 directional 2 dimensions principal component analysis technique. Thus, the data redundancy was efficiently decreased by the scheme, along it was more feasible. A RR over 99% was attained by the scheme, as shown by the investigational findings; however, the system needed higher computational power.

III. Proposed Finger Vein Authentication of The User Data

An effective biometric method that recognizes individuals utilizing their unique FV patterns is FVR. Amongst these, FVR possesses the subsequent advantages: (1) FV identification makes it complicated to falsify or steal identification since veins are concealed within the body and are mainly unseen to the naked eye; (2) both convenience and also cleanliness are ensured by the non-invasive along with contactless capture, thereby the system is created more apt for the user. But, FV identification is impacted by performance degradation resulting from illumination variations, information loss produced during feature pattern extraction, as well as reduction and misclassification error upon image capture. For addressing the above issues, an ES-RwCNN is created by the work for executing the user data's FV authentication, as exhibited in Fig 1.

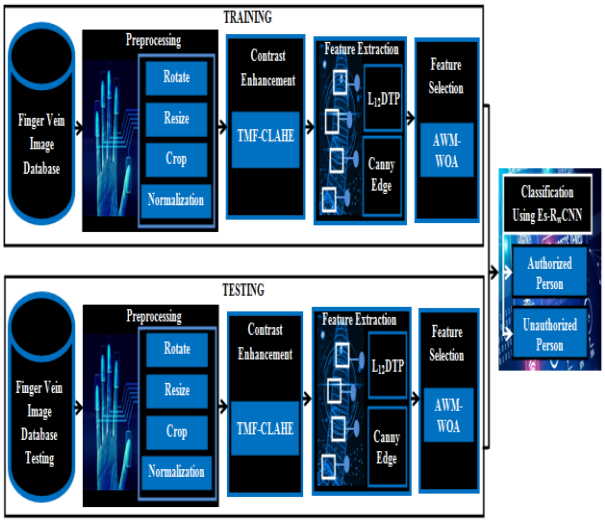

Fig 1: Proposed ES-RwCNN to perform the finger vein authentication of the user data

A. TRAINING PHASE AND TESTING PHASE

Utilizing the developed classification model namely ES-RwCNN for recognizing the FV, various sampled images

are separated into trained and tested images and processed. Disparate phases of processing namely pre-processing, CE, FE, along with feature selection (FS), is undergone by the compilation of split-sample trained and tested images for improvising the classification outcome to identify the FV.

Pre-processing

By addressing the challenges faced on account of the unwilling distortions, the image's image rotation (P_1^{rot}), resizing (P_2^{resize}), cropping (P_3^{crop}), along normalization ($\mathrm{P}_4^{normalize}$) are executed by pre-processing. The error chances are evaded by pre-processing and improvising the RR.

$$\mathrm{P}_1^{rot} = \Re_{i,j}^{rot}\left[\Gamma_{i,j}\right] \quad (1)$$

$$\mathrm{P}_2^{resize} = \Re_{i,j}^{resize}\left[\Gamma_{i,j}\right] \quad (2)$$

$$\mathrm{P}_3^{crop} = \Re_{i,j}^{crop}\left[\Gamma_{i,j}\right] \quad (3)$$

$$\mathrm{P}_4^{normalize} = \Re_{i,j}^{normalize}\left[\Gamma_{i,j}\right] \quad (4)$$

Wherein $\Gamma_{i,j}$ implies the input image, $\Re_{i,j}^{rot}$ $\Re_{i,j}^{resize}$ $\Re_{i,j}^{crop}$ along with $\Re_{i,j}^{normalize}$ demonstrates the pre-processing functions that execute rotation, resizing, cropping, and normalization.

Contrast Enhancement

The information's perception in the image is enhanced through the CE phase. A superior result is offered by arresting the uneven shading along with vein posture deformation that degrades the FV authentication accuracy. An enhancement technique called TMF-CLAHE is created by the work. Trapezoid Membership Function (TMF) is applied by the TMF-CLAHE method for automatic determination of clipping-parameter that restricts the contrast level in an image, therefore, causing an enhanced image (EI). For attaining the EI, the proposed TMF-CLAHE comprises the subsequent steps:

Step1: Firstly, convert the OI intensity level into the contextual regions, which don't overlap. This region is called an image tile of dimension $\mathrm{A}\times\mathrm{B}$.

Step2: By creating the textual region's histogram in the dimensional space $\mathrm{A}\times\mathrm{B}$, the respective region is assessed.

Step3: The contextual region is gauged along with restricted with a *CL* (clipped limit) value-centered upon the histogram, such as

$$\mathrm{B}_{avg} = \frac{(\mathrm{B}_\Gamma x \times \mathrm{B}_\Gamma y)}{\mathrm{B}_{grey}} \quad (5)$$

Wherein B_{avg} indicates the pixel's average number, B_{grey} symbolizes the grey levels in the contextual region, $\mathrm{B}_\Gamma x$ and $\mathrm{B}_\Gamma y$ signifies the pixel values along the x and also y directions inside the contextual regions. Now, utilizing the TMF, the images' over enhancement along with under enhancement is lessened by establishing the predetermined clip limit, which was a primary challenge whilst fixing a pre-fixed clip limit. Therefore, the clipping parameter attained is disparate as of the image upon which TMF-CLAHE is implemented that is presented as:

$$\vartheta_\Gamma(\mathrm{B}_{CL}) = \begin{cases} 0 & if\ (\mathrm{B}_{CL} \le a)\ o\ (\mathrm{B}_{CL} \ge d) \\ (\mathrm{B}_{CL} - a)/(b-a) & if\ \mathrm{B}_{CL} \in (a,b] \\ 1 & if\ \mathrm{B}_{CL} \in (b,c] \\ (d - \mathrm{B}_{CL})/(d-c) & if\ \mathrm{B}_{CL} \in (b,d] \end{cases} \quad (6)$$

Wherein $\vartheta_\Gamma(\mathrm{B}_{CL})$ signifies the image's clipping parameter, which is dependent, (a,b,c,d) shows the trapezoidal membership function (T_F) 's coordinates.

Hence, the clip limit is measured by the TMF, and the computed clip limit is changed on the predefined crisp clip limit. Now, the actual CL is specified as:

$$\mathrm{B}_{CL} = \mathrm{B}_{Clip} \times \mathrm{B}_{avg} \quad (7)$$

Here, by specific conditions, the pixel's clipping is decided; that are, the corresponding pixels get clipped if B_{CL} is lesser than a number of pixels in a specific limit of array [0, 1]. Now, that pixel's average location is decided as $\mathrm{B}_{\sum clip}$, and for every gray-level, the remaining pixel's average is distributed as:

$$\mathrm{B}_{avggray} = \frac{\mathrm{B}_{\sum clip}}{\mathrm{B}_{gray}} \quad (8)$$

The subsequent statements present the theory of trimming histograms:

$$\begin{aligned} &if \aleph_{region}(i) = \mathrm{B}_{CL} \\ &\aleph_{region_{clip}}(i) = \mathrm{B}_{CL} \\ &Else\ if\left(\aleph_{region}(i) + \mathrm{B}_{avggray}\right) > \mathrm{B}_{CL} \\ &\aleph_{region_{clip}}(i) = \mathrm{B}_{CL} \\ &else\ \aleph_{region_{clip}}(i) + \aleph_{region}(i) = \mathrm{B}_{CL} \end{aligned} \quad (9)$$

Whereas $\aleph_{region}(i)$ and $\aleph_{region_{clip}}(i)$ symbolizes the original grey-level histograms along with trimmed histograms of every region at i^{th} gray-level.

Step5: The remaining pixels are rearranged until every pixel has been allotted. The pixel step's rearrangement is proffered by: $step = \mathrm{B}_{gray} / \mathrm{B}_{remain}$

B_{remain} implies the remaining number of clipped pixels. The steps are repeated till every pixel gets distributed uniformly. The vein's important selection is offered by the TMF-CLAHE CE, where the ridges are observable and

distinguishable to each other along with deeming it the ROI of FV image.

Feature Extraction

For offering the FV's knowledge to the classification model, the features (relevant) are extracted via FE. For decreasing the CC, FE assists the model along with helping for precise personal identification systems. Utilizing L_{12}DTP and also Canny edge techniques, textural and EFs are extracted as of the EI by the proposed work. The developed extraction technique can extract both local and also global features comprising micro-patterns.

a. Local 12 direction texture pattern (L_{12}DTP)

Using L_{12}DTP, the texture-centered feature is extracted that separates the image into 13x13 regions. The divided region is measured along with the numerous directions, like 0°, 15°, 30°, 45°, 60°, 75°, 90°, 105°, 120°, 135°, 150°, and 165° centered upon the magnitude along with sign. Therefore, the center pixel's 12 diagonal directions in an image are formed by the pixel value. Then, by contrasting each pixel with the nearest neighboring pixel within the same direction, the 13 × 13 regions are assessed for sign operation (T_{θ_i}) as signified below

$$\mathrm{T}_{\theta_i}=\sum_{k=0}^{k-2}\mu\left(\chi_p-\chi_{p+1}\right)2^k k \tag{10}$$

$$\theta_i=0^{\bullet},15^{\bullet},30^{\bullet},45^{\bullet},60^{\bullet},75^{\bullet},90^{\bullet},105^{\bullet},120^{\bullet},135^{\bullet},150^{\bullet},165^{\bullet}$$

$$\mu(\Gamma^*)=\begin{cases}1, & \Gamma^*\geq 0\\ 0, & otherwise\end{cases} \tag{11}$$

Wherein, k symbolizes the number of neighbors and θ_i characterizes the 12 directions.

Then, by analyzing the nearby absolute differences values and a global threshold, the magnitude (M_{θ_i}) is estimated. The magnitude mathematical formulation is presented below:

$$M_{\theta_i}=\sum_{k=0}^{k-2}\mu\left(\left|\chi_p-\chi_{p+1}\right|-\alpha\right)2^k \tag{12}$$

$$\theta_i=0^{\bullet},15^{\bullet},30^{\bullet},45^{\bullet},60^{\bullet},75^{\bullet},90^{\bullet},105^{\bullet},120^{\bullet},135^{\bullet},150^{\bullet},165^{\bullet}$$

$$\alpha=\frac{1}{k-1}\sum_{k=0}^{k-2}\mu\left(\chi_p-\chi_{p+1}\right). \tag{13}$$

The entire image is signified by creating a histogram after calculating T_{θ_i} and M_{θ_i} as

$$hist(\mathrm{T}_{\theta_i}(l))=\sum_{i=1}^{A}\sum_{j=1}^{B}F_2\left(\mathrm{T}_{\theta_i}(i,j),l\right) \tag{14}$$

$$l\in\left[0,\left(2^k-1\right)\right] \tag{15}$$

$$hist(M_{\theta_i}(l))=\sum_{i=1}^{A}\sum_{j=1}^{B}F_2\left(M_{\theta_i}(i,j),l\right) \tag{16}$$

$$F_2(\Gamma_i,\Gamma_j)=\begin{cases}1 & \Gamma_i=\Gamma_j\\ 0 & otherwise\end{cases} \tag{17}$$

Wherein $\mathrm{A}\times\mathrm{B}$ symbolizes the input image's size and k represents the total neighbors. Lastly, the concatenation of two histograms and extraction of features is done.

$$hist_{concat}=\left[hist(\mathrm{T}_{\theta_i}(l));hist(M_{\theta_i}(l))\right] \tag{18}$$

b. Canny Edge

Different features linked to edges or boundaries are measured by Canny Edge Detector. An extra advantage is offered by EF via enhancing the FVR detection with huge accuracy.

Firstly, for removing the unnecessary details, the image is processed in a Gaussian filter, i.e., provided as:

$$e\left(\Gamma_i,\Gamma_j\right)=E\left(\Gamma_i,\Gamma_j\right)*F\left(\Gamma_i,\Gamma_j\right) \tag{19}$$

$$E=\frac{1}{\sqrt{2\pi\alpha^2}}\exp\left(-\frac{\Gamma_i^2+\Gamma_j^2}{2\alpha^2}\right) \tag{20}$$

Then, the gradient is measured for gradient operations:

$$G\left(\Gamma_i,\Gamma_j\right)=\sqrt{\kappa_i^2(\Gamma_i,\Gamma_j)+\kappa_j^2(\Gamma_i,\Gamma_j)} \tag{21}$$

$$\theta\left(\Gamma_i,\Gamma_j\right)=\tan^{-1}\left[\kappa_i\left(\Gamma_i,\Gamma_j\right)/\kappa_j\left(\Gamma_i,\Gamma_j\right)\right] \tag{22}$$

After that, for suppressing every noisy data as of the selected edge data, a threshold value is estimated.

$$G_T\left(\Gamma_i,\Gamma_j\right)=\begin{cases}G(\Gamma_i,\Gamma_j), & if\ G(\Gamma_i,\Gamma_j)>T\\ 0, & otherwise\end{cases} \tag{23}$$

Wherein T implies the selection in which every edge element are kept whilst numerous noise is repressed.

Next, for attaining a thin edge ridge, the chosen edge data G_T is suppressed. By checking whether each non-zero $G(\Gamma_i,\Gamma_j)$ is larger contrasted to its 2 neighbors along the gradient direction $\theta\left(\Gamma_i,\Gamma_j\right)$, each edge is assessed for thinning the edges. If so, it is kept unchanged otherwise, fix it to 0.

For obtaining 2 binary images ς_1 and ς_2, two disparate thresholds are fixed τ_1 and also τ_2 for the preceding result. There exists less noise and also fewer false borders while ς_2 is contains a larger threshold τ_2 but has a limitation of wide edge tolerance as analogized to ς_1 with a smaller threshold τ_1 .

Numerous features are calculated centered upon the edge. Therefore, a collection of features, i.e. the textural and also EF, is saved within the data frame.

Feature Selection

The most significant and informative features are extracted by the FS, which enhances the improved performance in FVR. AWM-WOA has been formed by the work for better FS. The CC is effectively mitigated by the created algorithm. Thus, the classification model's accuracy is improved with limited time and cost. The optimal solution

(OS) is attained by the AWM-WOA grounded on the developed objective function that chooses the more informative feature that is offered by a sum of disparate features and forms a sole objective function formulated as:

$$\xi_{objective}(\Gamma_E^*) = \xi_1(\Gamma_1^*) + \xi_2(\Gamma_2^*) + \xi_3(\Gamma_3^*) + ...+ \xi_n(\Gamma_n^*) \quad (24)$$

Wherein $\xi_1, \xi_2, ...\xi_n$ symbolizes the constant value that provides the polarity of the features $\Gamma_1^*, \Gamma_2^*, \Gamma_3^* \ldots\ldots \Gamma_n^*$.

Step 1: Firstly, the present best search agent's position is presumed as an optimum point. The other search agents update their position centered upon the best search agent-centered on the optimum point. This equation is provided as:

$$\vec{\vartheta} = \left|\vec{k}.\overrightarrow{\Gamma_n^{\chi}}(t) - \overrightarrow{\Gamma_n^*}(t)\right|, \quad (25)$$

$$\overrightarrow{\Gamma_n^*}(t+1) = \overrightarrow{\Gamma_n^{\chi}}(t) - \vec{\alpha}.\vec{\vartheta}, \quad (26)$$

Where t symbolizes the existing iteration, $\overrightarrow{\Gamma_n^{\chi}}$ implies the best solution's n^{th} position vector, $\overrightarrow{\Gamma_n^*}$ implies the n^{th} position vector of every agent along with $\overrightarrow{\Gamma_n^*}(t+1)$ symbolizes the updated position. $\vec{\alpha}$ along with's coefficients are gauged as

$$\vec{\alpha} = 2.\vec{a}.r - \vec{a} \quad (27)$$

$$\vec{k} = 2r \quad (28)$$

Where, a is slowly reduced as of 2 to 0 and r signifies a random number at the interval [0, 1].

Step 2: The exploitation assures the searching of OS inside the limited space in this step. Further, two disparate phases are undergone by the exploitation process that is described below:

Phase 1: $\vec{\alpha}$ implies a random value within the interval $[-a, a]$ in, which a reduces as of 2 to 0 over the iterations in this phase. The new search agent position could be stated betwixt the position (original) together with the agent's updated position by setting the arbitrary values for $\vec{\alpha}$ within the interval [-1, 1]. The best OS is not attained because the updated solution gets converged over the local optimal search space. For balancing this, the whale optimization merges with the Adaptive weight factor, which is dynamically modified with iteration number that sustains the global along with local searchability. The adaptive search scope grounded on the inertia weight function w is articulated as:

$$\begin{cases} \Lambda = w \times \vec{\vartheta} \times (rand(0,1) - 0.5) \\ w = \exp(-x_1 \times (I / I_m)^{x_2}) \end{cases} \quad (29)$$

Wherein, x_1 along with x_2 in the gamut of [1, 30] are the predefined constants for modifying the search scope, present iteration, together with the maximum iteration, is indicated as I and I_m correspondingly.

Phase 2: A spiral equation is formed betwixt the whale and also prey's position that is offered as

$$\overrightarrow{\vartheta^t} = \left|\overrightarrow{\Gamma_n^{\chi}}(t) - \vec{\Gamma}_n^*(t)\right| \quad (30)$$

$$\overrightarrow{\Gamma_n^*}(t+1) = \overrightarrow{\vartheta^t} e^{gl}.\cos(2\pi l) + \overrightarrow{\Gamma_n^{\chi}}(t) \quad (31)$$

Where the distance betwixt the whale along with prey is signified as ϑ^t, g implies a constant that signifies the logarithmic shape, l denotes a random value within the interval [-1, 1].

The spiral model movement is simulated throughout the algorithm's iterations that are proffered as.

$$\overrightarrow{\Gamma_n^*}(t+1) = \begin{cases} \overrightarrow{\Gamma_n^{\chi}}(t) - \vec{\alpha}.\vec{\vartheta} & if \quad p < 0.5; \\ \vec{\vartheta} e^{gl}.\cos(2\pi l) + \overrightarrow{\Gamma_n^{\chi}}(t) & if \quad p \geq 0.5, \end{cases} \quad (32)$$

(32))

Wherein, p implies a random number in [0, 1].

Step 3: The exploration stage is conducted, which assures the searching of the OS in a broad variety of areas in step 3. The exploration stage is contrary to the exploitation stage. In step 2 $\vec{\alpha}$ is presumed as a random value that is larger analogized to 1 or smaller than -1 in an interval [-1, 1]. The search agent's position might remain distant from the whale together with its position is updated utilizing the novel mutation operator. The new offspring's diversity is enhanced by this application and assists WOA to jump out of local optima. The searching process continues from the existing solution $\overrightarrow{\Gamma_n^*}(t)$ to its nearest solution Γ_{SN} centered on the novel mutation operator.

$$\overrightarrow{\Gamma_n^*}(t) = \overrightarrow{\Gamma_n^*}(t) + \phi_t(\overrightarrow{\Gamma_n^*}(t) - \Gamma_{SN}) \quad (33)$$

Where $t \in \{1,2,3....., SN/2\}$ signifies a random index, SN implies the populace size, and $\phi_{i,j}$ signifies a random integer $[-1,1]$.

The updated solution's position is formulated as:

$$\vec{\vartheta} = \left|\vec{k}.\overrightarrow{\Gamma_n^*}(t) - \overrightarrow{\Gamma_n^*}\right| \quad (34)$$

$$\overrightarrow{\Gamma_n^*}(t+1) = \overrightarrow{\Gamma_n^*}(t) - \vec{\alpha}.\vec{\vartheta} \quad (35)$$

Wherein Γ_n^* is an updated position vector.

In the objective solution, the attained solution is substituted; the top solution is elected as the most instructive feature. Thereafter, it is kept in a set as stated below:

$$\xi(\Gamma_E^*) = \left\{\Gamma_1^* + \Gamma_2^* + \Gamma_3^* + ... + \Gamma\right\}_n^* \quad (36)$$

B. CLASSIFICATION

For detecting precisely whether the finger-vein is authorized or unauthorized, classification is useful. Generally, for attaining a superior classification score, the NN is mostly utilized. Whilst performing back-propagation, a vanishing gradient (VG) takes place that causes slow-down learning and also decreases the classification rate. For solving this issue, an Es-RwCNN is formed by the work for enhancing the CA for FVR.

Over the chosen features, the developed ES-RwCNN gets trained. Afterward, they are tested to compute the classification score for identifying finger veins. For obtaining training and attaining the recognition, that is if the person is authorized or not, the sample features are processed inside numerous layers. The convolution layer (CL), relu layer, pooling layer (PL), and also fully connected layer (FCL) are the layers.

1) Convolutional Layer: A set of two-dimensional convolutions betwixt the input features Γ_m^l is executed by the CL, where l and m symbolizes the levels and map indexes and the kernel filter K_m^l, i.e. provided as $\left[\Gamma_m^l\right]\times \mathrm{K}_m^l$. After filtration, the n^{th} output map $\hat{\lambda}_n^l$ attained by the CL is measured as

$$\hat{\lambda}_n^l = \sum_{i=0}^{n}\sum_{j=0}^{n} w_{i,j}^l \Gamma_{i,j}^l + \mathrm{B}_{i,j}^l \quad (37)$$

(37

Wherein i, j indicates rows and also columns that signify the features, $w_{i,j}^l$ signifies the weight at the respective interval of l, $\mathrm{B}_{i,j}^l$ implies the bias of interval of l

2) ReLU: For studying the features, an activation function (AF) that decides which neurons must be trained or activated is Relu (act_{relu}). It supports the system's nonlinearity, and the VG issue is decreased. It enables the network's quicker training without sacrificing accuracy. The ReLU activation is proffered as:

$$f\left(\Gamma_m^l\right) = \max\left[0, \Gamma_m^l\right] \quad (38)$$

This layer is united with the CL and deals with augmenting the model's nonlinear properties and also the total network without influencing the receptive fields of the CL i.e.

$$\hat{\lambda}_n^l = act_{relu}\left(\sum_{i=0}^{N}\sum_{j=0}^{N} w_{i,j}^l \Gamma_{i,j}^l + \mathrm{B}_{i,j}^l\right) \quad (39)$$

(39)

3) Pooling: An approach aimed at down sampling the feature map is presented by the PL by summarizing a feature's existence in patches of the feature map. By decreasing dimensionality, the calculation power needed for processing the data is lessened. Whilst efficiently preserving the model's training, it is employed for extracting invariant dominant rotational and positional features.

$$\lambda_n^p = \forall_{layers}^{+}\left(\left|\Gamma_m^l\right|\right) \quad (40)$$

Wherein $\forall_{layers}^{+}$ might symbolize disparate PLs, like maximum PL, minimum PL, average PL, etc. For improvising the image's quality, the PL is helpful.

A CNN's i^{th} layer is formed by the CL and the PL. For capturing the low-level information much more depending upon the image's complexity, the number of such layers could be augmented. Therefore, the output from the CL is flattened and further preceded.

$$\aleph_3^{pooling}(F_{Flatten}) = \left[\Im_1, \Im_2, \Im_3, \Im_4, ... \Im_n\right] \quad (41)$$

4) Fully Connected Layer: An N-dimensional vector is generated, where N implies the total classes that the program has to select as of the flattened features. For categorizing the image (input) affiliated to a particular label, a Sigmoid AF (act_σ) is normally utilized. In FCL, the VG's drawback is possessed by the sigmoid function that generally occurred during the back-propagation method causing slow-down learning and also a reduction in classification rate. By mitigating saturation to lessen the VG issue within the network, Enhanced Sigmoid (ES) AF is designed overcome this issue. It attains superior results for classification. Let Γ_m implies the m^{th} input map of the output layer Θ_m^l. Next, the linear combination Θ_m^l is specified as:

$$\Theta_m^l = act_\sigma\left(\sum_{i=1}^{n} w_i \Im_{i,j} + \mathrm{B}_{i,j}\right) \quad (42)$$

$$\dot{f}_m'(\Gamma_m) = \begin{cases} \beta\left(\Gamma_m - a\right) + act_{E\sigma}(a) & \Gamma_m >= a \\ act_{E\sigma}(a) & -a < \Gamma_m < a \\ \beta\left(\Gamma_m + a\right) + act_{E\sigma}(a) & \Gamma_m \le -a \end{cases} \quad (43)$$

$$\dot{f}_m''(\Gamma_m) = \begin{cases} \beta & \left|\Gamma_m\right| >= a \\ act_{E\sigma}'(\Gamma_m) & \left|\Gamma_m\right| < a \end{cases} \quad (44)$$

Where, $\dot{f}_m'(\Gamma_m)$ signifies the ES function, $\dot{f}_m''(\Gamma_m)$ represents the derivative function, and where a indicates the threshold and β signifies the slope, both parameters are preset.

The classification result is proffered by the FCL. Thereafter, for obtaining a precise result, the loss function (LF) is calculated. The LF is assessed betwixt the actual value (Γ_i) and the predicted value ($\hat{\Gamma}_i$) that is provided as:

$$\lambda_n^{loss} = \sum\left(\Gamma_i - \hat{\Gamma}_i\right)^2 \quad (45)$$

For the optimization of weight function, the re-weighted LF is measured that is offered as:

$$w_n^{(t+1)} = w_n^t + \frac{\eta\nu}{mn}\sum_{i=1}^{m}\sum_{j=1}^{n} \forall_{\phi_j} \wp_{v_j} \forall_{\phi} \wp_i \left(a \lg\left(\theta, D_i^S\right)\right)^T \quad (46)$$

(4

Wherein, $w_n^{(t+1)}$ signifies the updated weights, w_n^t implies the current weights, η is a meta objective step size, ν is the weight update step size, $\forall_{\phi_j} \wp_{v_j}$ symbolizes the training feature's validation, $\forall_{\phi}\, \wp_i$ indicates the validation of the

tested features, $a\lg(\theta, D_i^S)$ demonstrates the weight's gradient descent.

Finally, the misclassification error is lessened by the reweighted loss for the CA enhancement aimed at FVR. Hence, Fig 2 exhibits the proposed ES-RwCNN's overall outline in pseudo-code.

Input: Extracted features $F_{EXT}^{'} = \left[\xi_1^+, \xi_2^+, \xi_3^+, \xi_4^+, \ldots, \xi_N^+\right]$

Output: Finger Vein Recognition (authorized person or unauthorized person)

Begin

Initialize the kernel (K_m^l), bias $(B_{i,j}^l)$, pooling layer $(\forall_{layers}^+)$, weights $w_{i,j}^l$

For κ features in dataset

Evaluate the convolution operation using,

$$\lambda_n^l(\kappa) = \sum_{i=0}^{n}\sum_{j=0}^{n} w_{i,j}^l \Gamma_{i,j}^l + B_{i,j}^l$$

Compute the convolution layer with activation function

$$\lambda_n^l = act_{relu}\left(\sum_{i=0}^{N}\sum_{j=0}^{N} w_{i,j}^l \Gamma_{i,j}^l + B_{i,j}^l\right)$$

Generate pooling layer,

$$\lambda_n^p = \forall_{layers}^+\left(\Gamma_m^l\right)$$

Evaluate the fully connected layer using,

$$\Theta_m^l = act_{Z\sigma}\left(\sum_{i=1}^{n} w_i \Im_{i,j} + B_{i,j}\right)$$

If $\left(\sum\left(\Gamma_l - \hat{\Gamma}_l\right)^2 = 0\right)$

Accurate finger vein recognition

If $\left(\hat{\Gamma}_i > 0.5\right)$

Output as Authorized person

Else

Output as Unauthorized person

End if

Else

Update weights using,

$$w_n^{(i+1)} = w_n^l + \frac{\eta\nu}{mn}\sum_{i=1}^{m}\sum_{j=1}^{n} \forall_{\phi_i}\varphi_{\nu_j}\forall_{\phi_j}\varphi_i\left(a\lg\left(\theta, D_i^S\right)\right)^T$$

End if

End for

End begin

Fig 2: Pseudo-code for proposed ES-RwCNN

IV. Results

Centered on different performance metrics for the FVR, the complete analysis of the proposed framework's final outcome with prevailing methods is elucidated here. For stating the proposed method's efficiency, both the performance analysis and also comparative analysis are executed. The proposed technique is implemented in MATLAB with machine configuration of Intel core i7 processor, 3.20 GHz CPU Speed, windows 7 OS. The data are amassed from the openly accessible dataset.

A. Performance Analysis

Centered upon different evaluation metrics, the proposed work's brief analysis was executed. Besides, a comparative review is also conducted. For the pre-processing model TMF-CLAHE and also the classification model ES-RwCNN, the analysis is executed.

1. Performance Analysis of Proposed Preprocessing Technique

Concerning disparate performance metrics, like Correlation, Image Quality Index (IQI), and Spearman Rank Correlation (SRC) with different prevailing methods like CLAHE, Histogram Equalization (HE), and Bi-lateral filtering method, the proposed TMF-CLAHE's performance analysis is validated. Next, to illustrate its efficiency, a comparative study was conducted. Table I tabulates the metric's evaluation.

TABLE I
Performance analysis of proposed TMF-CLAHE based on Correlation, Image Quality Index, and Spearman Rank Correlation

Performance metrics/Techniques	Correlation	Image Quality Index	Spearman Rank Correlation
Proposed TMF-CLAHE	0.971	0.799	0.998
CLAHE	0.940	0.583	0.939
Histogram Equalization	0.850	0.036	0.888
Bi-lateral Filtering	0.941	0.000	0.940

The performance analysis concerning the proposed TMF-CLAHE's correlation, IQI, and also SRC with different existent techniques, namely CLAHE, HE, and Bi-lateral filtering technique, is assessed in Table I. The similarities betwixt the EI and the OI are denoted by correlation. The similarities betwixt the EI and the OI with minimum information loss are denoted by the higher correlation rate. As per that, 0.971 correlations betwixt the images are attained by the proposed TMF-CLAHE, while the existing method obtains a 0.91 average correlation, which is moderately less as analogized to the existent techniques.

Furthermore, the SRC is also deemed. The degree of association betwixt the EI and the OI is quantified by the SRC. The higher Spearman correlation characterizes the better model and also vice versa. Thus, a higher SRC of 0.998 is displayed by the TMF-CLAHE proposed, but the prevailing methods acquire an average of 0.922 SRC, which is moderately less when weighted against the proposed one. Therefore, the proposed TMF-CLAHE is more effectual, together with the image is delivered at the higher-quality index at the rate of 0.799, whilst 0.583, 0.036, and 0.000 are attained by the prevailing techniques, like CLAHE, HE, and also Bi-lateral filtering technique correspondingly. Therefore, a quality image with no distortion is offered by the proposed TMF-CLAHE.

Fig 3 demonstrates the proposed TMF-CLAHE's graphical analysis with different existing methods, namely CLAHE, HE, and the Bi-lateral filtering technique. It is obviously known from figure 3 that a greater range of correlation, IQI, and SRC is attained by the TMF-CLAHE. The proposed method's high correlation is shown in figure 3 (a); thus, the uneven detection could be effortlessly rectified. Fig 3 (b) exhibits the IQI, which assists in clear image delivery. The SRC is exhibited in Fig 3 (c), which offers a precise association rate. These metrics measure the proposed TMF-CLAHE's effectiveness. Thus, the proposed TMF-CLAHE surpasses the existing technique.

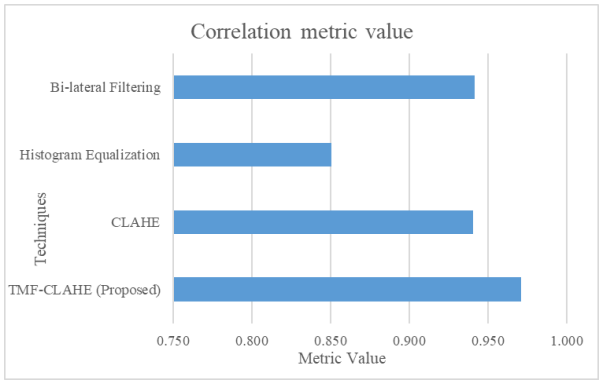

(a)

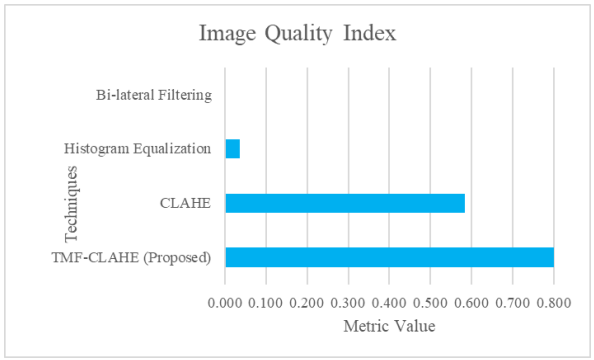

(b)

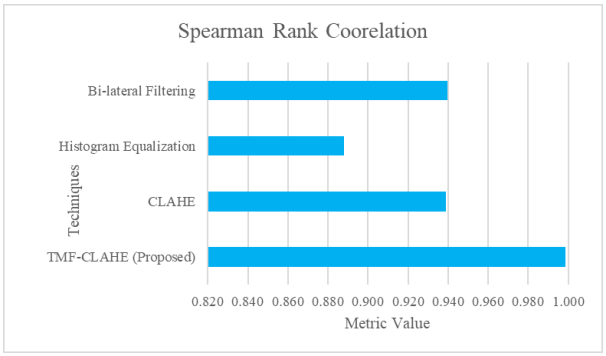

(c)

Fig 3: Graphical Demonstration of proposed TMF-CLAHE based on (a) Correlation, (b) Image Quality Index and (c) Spearman Rank Correlation.

B. Performance Analysis of Proposed Classification Technique:

Concerning disparate performance metrics, namely specificity, sensitivity, accuracy, Negative Predictive Value (NPV), recall, precision, F-Measure, Matthews Correlation Coefficient (MCC), FPR, and FRR, the proposed ES-RwCNN's performance analysis is validated. Afterward, a comparative study is conducted with prevailing methods, like Deep NN (DNN), Convolutional DNN (CDNN), along with Artificial NN (ANN). Tables II, III, and also IV tabularizes the metric's evaluation.

Table II:
Performance analysis of proposed ES-RwCNN based on sensitivity, specificity, accuracy, and NPV

Performance metrics/Techniques	Sensitivity	Specificity	Accuracy	NPV
Proposed ES-RwCNN	97.64	96.46	97.05	97.61
DNN	88.21	84.67	86.44	87.78
CDNN	90.57	91.75	91.16	90.68
ANN	69.81	42.22	56.01	58.31

Table II illustrates the different performance metrics' analysis, like specificity, NPV, accuracy, and also the sensitivity of the ES-RwCNN proposed with the various prevailing techniques, like DNN, CDNN, and ANN. The evaluation metrics must stand with a greater metrics rate for alleviating the VG issue within the network. According to that, the ES-RwCNN proposed attaining the sensitivity, specificity, accuracy, and NPV at the rate of 97.64%, 96.46%, 97.05%, and 97.61%, correspondingly, which overall ranges betwixt 96.46% to 97.64%. However, the metrics' value that overall ranges between 42.22%-91.75% are attained by the prevailing techniques, like DNN, CDNN, and ANN, which is relatively low when weighted against the proposed ES-RwCNN. Hence, the authorized along with the unauthorized person are efficiently distinguished by employing the proposed ES-RwCNN in the FVR.

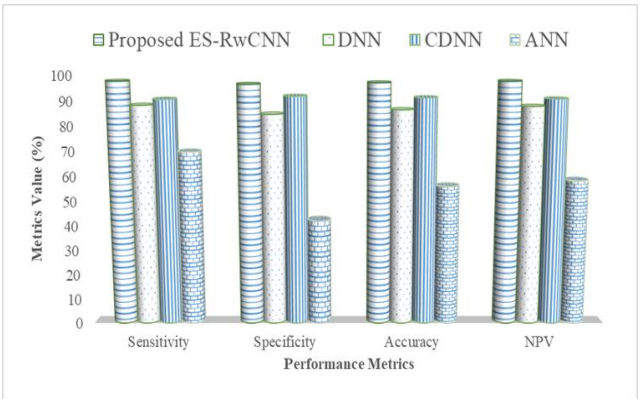

Fig 4: Graphical representation of the proposed ES-RwCNN based on sensitivity, specificity, accuracy, and NPV

Fig 4 exhibits the graphical depiction of the proposed ES-RwCNN's performance analysis with the disparate prevailing techniques, namely DNN, CDNN, and ANN. It is evidently known as of the figure that a superior performance metrics value is gained by means of the proposed one. Thus, the proposed ES-RwCNN surpasses several prevailing ones and offers precise FVR in disparate situations.

TABLE III
Performance analysis of proposed ES-RwCNN based on precision, recall and F-Measure

Performance metrics/Techniques	Precision	Recall	F-Measure
proposed ES-RwCNN	96.5	97.64	97.07
DNN	85.19	88.21	86.67
CDNN	91.65	90.57	91.1
ANN	54.71	69.81	61.35

Grounded upon the metrics of precision recall, along with F-Measure, Table III exhibits the proposed ES-RwCNN's evaluation. These metrics are mainly significant in the LF's prediction. The misclassification error is lessened by the LF for the CA enhancement for FVR. It is detected as of the table that 96.5% precision, 97.64% recall, and 97.07% F-Measure are attained by the ES-RwCNN proposed, which is relatively larger analogized to the prevalent technique. Thus, the existent method, like DNN, CDNN, and ANN attains the metrics' value that overall ranges from 54.71%-91.65%. Therefore, the FV is detected by the proposed one by overcoming the uncertainties along with a reduced error rate as contrasted to the prevailing model.

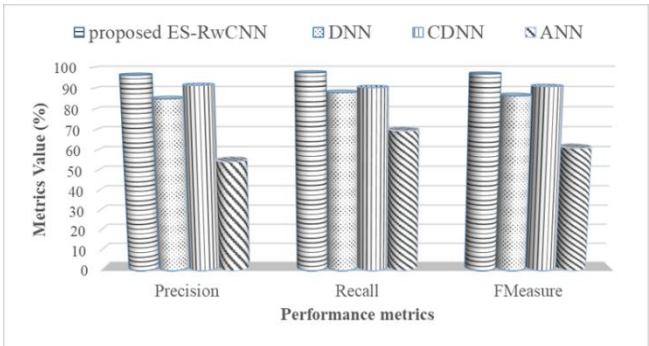

Fig 5: Graphical representation of the proposed ES-RwCNN based on precision, recall, and F-Measure.

The graphical illustration, which relatively examines the proposed ES-RwCNN with the prevailing methods, say DNN, CDNN, and ANN, is exhibited in Fig 5. The proposed ES-RwCNN is more effectual when contrasted to the prevalent methods, as stated by the comparative study. Hence, the uncertainties with the decreased error rate are effectively addressed by the proposed ES-RwCNN whilst the existing technique failed to manage such uncertainties.

TABLE IV
Evaluation of proposed ES-RwCNN based on MCC, FPR, and FRR

Performance metrics/Techniques	MCC	FPR	FRR
Proposed ES-RwCNN	94.11	3.53	2.35
DNN	72.92	15.33	11.79
CDNN	82.32	8.25	9.43
ANN	12.51	57.78	30.18

Centered upon the metrics of MCC, FPR, and FRR, Table IV depicts the proposed ES-RwCNN's performance analysis. The misclassification or miss-prediction error that happens in the FV's recognition is efficiently rejected by the lesser value of FPR and FRR. As per that, 3.53% FPR and 2.35% FRR are attained by the proposed one correspondingly. Contrarily, the high prediction rate is attained by the existing technique like DNN, CDNN, and ANN. FPR and FRR's average is 27.12% and 17.13%, correspondingly. Besides that, centered on MCC, the proposed ES-RwCNN is also deemed. The model's success is signified by a higher MCC score. Thus, the high MCC score of 94.11% is attained by the ES-RwCNN proposed, whilst the prevailing technique acquires the MCC score at an average of 60%. Hence, the slow convergence of triplet loss is conquered by the ES-RwCNN proposed and also assured the full usage of information with labels.

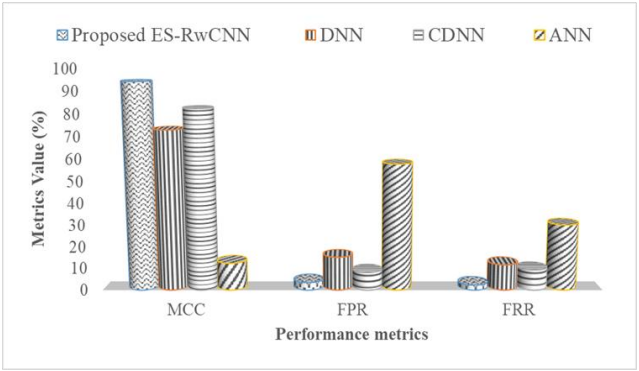

Fig 6: Graphical analysis of the proposed ES-RwCNN based on MCC, FPR, and FRR

The proposed ES-RwCNN's detailed analysis with different existing techniques, namely DNN, CDNN, and ANN is proffered in Fig 6. The best model is proffered by the illustration via examining the false prediction values. The false prediction is lessened by the proposed one and improvises the classification rate by evading misclassification and stays effective against the prevalent methods. Therefore, by attaining lower false prediction values and higher MCC scores, the proposed ES-RwCNN surpasses the prevailing methods.

V. Conclusion

A framework for detecting FV is formed by the work for safe authorization utilizing ES-RwCNN. Vein recognition is improved by the proposed framework via managing the challenge of unwilling distortions, diagonal pixel information, image variants, etc. In the TMF-CLAHE technique, the FV gets improved that concentrates upon irregular shading along with vein posture deformation and enhances the framework's accuracy. After that, utilizing the L_{12}DTP and also Canny Edge methods, relevant textural and EFs are extracted. Furthermore, AWM-WOA was applied by the work for removing the most knowledgeable feature which enhances accuracy along with lessens the CC. For identifying FV as an authorized or unauthorized person, the training along with testing is performed for the developed ES-RwCNN classification model. A low information loss is attained by the framework by attaining a 0.971 correlation betwixt the processed image and OI along with categorizes the FV with 97.05% accuracy, 97.64% sensitivity as shown by the experimental outcomes. The misclassification is evaded by employing the classification model via obtaining an FPR and FNR of 3.53% and 2.35%, correspondingly, and stays effective when weighted against the prevailing top-notch method.

References

[1] Antonio Iula, "Biometric recognition through 3D ultrasound hand geometry", Ultrasonics, vol. 111, pp. 1-24, 2021.
[2] Hui Ma and Zhang S. Y, "Contactless finger-vein verification based on oriented elements feature", Infrared Physics & Technology, vol. 97, pp. 149-155, 2019.
[3] Raid Rafi Omar Al-Nima, Mohammed AM Abdullah, Musab TS Al-Kaltakchi,Satnam Singh Dlay, WaiLok Woo and Jonathon A. Chambers, "Finger texture biometric verification exploiting multi-scale sobel angles local binary pattern features and score-based fusion", Digital Signal Processing, vol. 70, pp. 178-189, 2017.
[4] Yihua Shi Yang and GuiminJia, "Finger-vein image matching based on adaptive curve transformation", Pattern Recognition, vol. 66, pp. 34-43, 2017.
[5] Jian-DaWu and Chiung-Tsiung Liu, "Finger-vein pattern identification using principal component analysis and the neural network technique", Expert Systems with Applications, vol. 38, no. 5, pp. 5423-5427, 2011.
[6] ShirongQiu, Yaqin Liu, Yujia Zhou, Jing Huang and YixiaoNie, "Finger-vein recognition based on dual-sliding window localization and pseudo-elliptical transformer", Expert Systems with Applications, vol. 64, pp. 618-632, 2016.
[7] Huafeng Qin, Xiping He, Xingyan Yao and Hongbing Li, "Finger-vein verification based on the curvature in Radon space", Expert Systems with Applications, vol. 82, pp. 151-161, 2017.
[8] Kun Su, Gongping Yang, Bo Wu, Lu Yang, Dunfeng Li, Peng Su and Yilong Yin, "Human identification using finger vein and ECG signals", Neurocomputing, vol. 332, pp. 111-118, 2019.

[9] EuiChul Lee and Kang Ryoung Park, "Image restoration of skin scattering and optical blurring for finger vein recognition", Optics and Lasers in Engineering, vol. 49, no. 7, pp. 816-828, 2011.
[10] Shuyi Li, Bob Zhang, LunkeFei and Shuping Zhao, "Joint discriminative feature learning for multimodal finger recognition", Pattern Recognition, vol. 111, pp. 1-11, 2021.
[11] Kun Su, Gongping Yang, Lu Yang, Dunfeng Li, Peng Su and Yilong Yin, "Learning binary hash codes for finger vein image retrieval", Pattern Recognition Letters, vol. 117, pp. 74-82, 2019.
[12] Haiying Liu, Gongping Yang, Lu Yang and Yilong Yin, "Learning personalized binary codes for finger vein recognition", Neurocomputing, vol. 365, pp. 62-70, 2019.
[13] Fei Liu, Gongping Yang, Yilong Yin and Shuaiqiang Wang, "Singular value decomposition based minutiae matching method for finger vein recognition", Neurocomputing, vol. 145, pp. 75-89, 2014.
[14] Wenxiong Kang, Xiaopeng Chen and Qiuxia Wu, "The biometric recognition on contactless multi-spectrum finger images", Infrared Physics & Technology, vol. 68, pp. 19-27, 2015.
[15] Rama VasanthaAdiraju, Kranthi Kumar Masanipalli, Tamalampudi Deepak Reddy, RohiniPedapalli, SindhuChundru and Asisa Kumar Panigrahy, "An extensive survey on finger and palm vein recognition system", Materials Today: Proceedings, vol. 44, pp. 1-5, 2020.
[16] XianjingMeng, JinwenZheng, Xiaoming Xi, Qing Zhang and Yilong Yin, "Finger vein recognition based on zone-based minutia matching", Neurocomputing, vol. 423, pp. 1-16, 2021.
[17] Jian-Da Wu and Chiung-Tsiung Liu, "Finger-vein pattern identification using SVM and neural network technique", Expert Systems with Applications, vol. 38, no. 11, pp. 14284-14289, 2011.
[18] Dongdong Zhao, Hui Ma, Zedong Yang, Jianian Li and WenboTian, "Finger vein recognition based on lightweight CNN combining center loss and dynamic regularization", Infrared Physics & Technology, vol. 105, pp. 1-10, 2020.
[19] Yuxun Fang, Qiuxia Wu and Wenxiong Kang, "A novel finger vein verification system based on two-stream convolutional network learning", Neurocomputing, vol. 290, pp. 100-107, 2018.
[20] Mohsin A. H, Zaidan A. A, Zaidan B. B, Albahri O. S, Albahri A. S, Alsalem M. A and Mohammed K. I, "Based blockchain-PSO-AES techniques in finger vein biometrics: A novel verification secure framework for patient authentication", Computer Standards & Interfaces, vol. 66, pp. 1-25, 2019.
[21] Wenhao You, Weikang Zhou, Jing Huang, Feng Yang, Yaqin Liu and Ziyu Chen, "A bilayer image restoration for finger vein recognition", Neurocomputing, vol. 348, pp. 1-31, 2019.
[22] CihuiXieand Ajay Kumar, "Finger vein identification using convolutional neural network and supervised discrete hashing", In Deep Learning for Biometrics, Springer, Cham,vol. 119, pp. 1-31, 2017.
[23] Liu, Tong, JianbinXie, Wei Yan, Peiqin Li, and Huanzhang Lu, "Finger-vein pattern restoration with direction-variance-boundary constraint search", Engineering Applications of Artificial Intelligence, vol. 46, pp. 131-139, 2015.
[24] IsmailBoucherit, Mohamed OuldZmirli, HamzaHentabli and BakhtiarAffendiRosdi, "Finger vein identification using deeply-fused Convolutional Neural Network", Journal of King Saud University-Computer and Information Sciences, vol. 33, pp. 1-11, 2020.
[25] Weili Yang, Wei Luo, Wenxiong Kang, Zhixing Huang and Qiuxia Wu, "FVRAS-Net: an embedded finger-vein recognition and anti-spoofing system using a unified cnn", IEEE Transactions on Instrumentation and Measurement, vol. 69, no. 11, pp.1-12, 2020.
[26] Na Hu, Hui Ma and Tao Zhan, "Finger vein biometric verification using block multi-scale uniform local binary pattern features and block two-directional two-dimension principal component analysis", Optik, vol. 208, pp. 1-16, 2020.